Title

Infrasonic component of volcano-seismic eruption tremor

Journal

Geophys. Res. Lett., 41

Authors

Matoza, Robin S

Fee, David

Publication Date

2014-03-27

Peer reviewed

AGU PUBLICATIONS

Geophysical Research Letters

RESEARCH LETTER

10.1002/2014GL059301

Key Points:
- Volcanic eruption tremor contains air-ground coupled infrasound
- Subaerial eruption mechanism contributes to volcanic tremor
- Seismoacoustic cross correlation and cross-spectral analysis

Correspondence to:
R. S. Matoza,
rmatoza@ucsd.edu

Citation:
Matoza, R. S., and D. Fee (2014), Infrasonic component of volcano-seismic eruption tremor, *Geophys. Res. Lett.*, *41*, 1964–1970, doi:10.1002/2014GL059301.

Received 14 JAN 2014
Accepted 4 MAR 2014
Accepted article online 11 MAR 2014
Published online 27 MAR 2014

Infrasonic component of volcano-seismic eruption tremor

Robin S. Matoza[1] and David Fee[2]

[1]Institute of Geophysics and Planetary Physics, Scripps Institution of Oceanography, La Jolla, California, USA, [2]Wilson Infrasound Observatories, Alaska Volcano Observatory, Geophysical Institute, University of Alaska Fairbanks, Fairbanks, Alaska, USA

Abstract Air-ground and ground-air elastic wave coupling are key processes in the rapidly developing field of seismoacoustics and are particularly relevant for volcanoes. During a sustained explosive volcanic eruption, it is typical to record a sustained broadband signal on seismometers, termed eruption tremor. Eruption tremor is usually attributed to a subsurface seismic source process, such as the upward migration of magma and gases through the shallow conduit and vent. However, it is now known that sustained explosive volcanic eruptions also generate powerful tremor signals in the atmosphere, termed infrasonic tremor. We investigate infrasonic tremor coupling down into the ground and its contribution to the observed seismic tremor. Our methodology builds on that proposed by Ichihara et al. (2012) and involves cross-correlation, coherence, and cross-phase spectra between waveforms from nearly collocated seismic and infrasonic sensors; we apply it to datasets from Mount St. Helens, Tungurahua, and Redoubt Volcanoes.

1. Introduction

Volcanic tremor is a catchall term used for sustained seismic signals associated with a diverse range of volcanic activity [e.g., *McNutt*, 1992; *Chouet and Matoza*, 2013]. *Eruption tremor*, referring specifically to seismic volcanic tremor that occurs during eruptions, is typically a temporally varying broadband signal [*McNutt*, 2000; *McNutt and Nishimura*, 2008]. The source mechanism of eruption tremor has been attributed to the upward migration of magma and gases through the shallow conduit structure and vent [*McNutt and Nishimura*, 2008]. Eruption tremor has also been modeled as chaotic wagging of a magma column within a fragmenting and spatially heterogeneous annulus [*Jellinek and Bercovici*, 2011]. The low-frequency portion (0.5–1.5 Hz) of eruption tremor has been modeled as a downward vertical reaction force on the Earth in response to the thrust associated with expulsion of fluid from the vent [*Prejean and Brodsky*, 2011].

It is now well known that explosive volcanic eruptions also radiate large-amplitude acoustic signals (infrasound) directly into the atmosphere, with signals varying in duration between discrete explosion (blast) waveforms [e.g., *Firstov and Kravchenko*, 1996; *Johnson*, 2003; *Marchetti et al.*, 2013] and sustained, broadband, infrasonic tremor signals [e.g., *Vergniolle and Caplan-Auerbach*, 2006; *Matoza et al.*, 2009; *Fee et al.*, 2010; *Caplan-Auerbach et al.*, 2010]. In this paper, we investigate seismoacoustic coupling in data from volcanic eruptions. In two of three cases presented, seismic eruption tremor waveforms are found to contain air-to-ground coupled infrasonic tremor. An implication of our study is that care must be taken to identify and isolate the seismic (subsurface source) and acoustic (subaerial source) components of eruption tremor before modeling and interpreting them.

2. Methods

We build upon the method introduced by *Ichihara et al.* [2012], which considers the cross correlation between nearly collocated seismic and infrasonic sensors. *Ichihara et al.* [2012] analyzed changes in the pattern of the cross-correlation function $R[\tau; W(t, \mathbf{x_s}), P(t, \mathbf{x_p})]$ in sliding time windows, where $W(t, \mathbf{x_s})$ is the vertical seismic velocity waveform, $P(t, \mathbf{x_p})$ is the acoustic pressure waveform, τ is the lag time of W to P, t is time, and $\mathbf{x_s}$ and $\mathbf{x_p}$ are the locations of the seismometer and pressure sensor. According to *Ichihara et al.* [2012], in the presence of an energetic infrasound wave, this cross correlation is dominated by cross correlation between terms $p_{\text{in}}(t, \mathbf{x_p})$ and $H_{pw}p_{\text{in}}(t, \mathbf{x_s})$, where p_{in} is the incident pressure wave (in the atmosphere), and H_{pw} is the transfer coefficient from the incident pressure wave to vertical seismic velocity. A resultant characteristic pattern in the cross-correlation function can then be used to identify the component $R[\tau; H_{pw}p_{\text{in}}, p_{\text{in}}]$ and thereby identify incident infrasonic waves. This characteristic pattern ideally has a peak

at $\tau = 1/(4f_0)$, where f_0 is a characteristic frequency of the incident infrasound wave; this delay arises from a phase delay $e^{-i\pi/2}$ in H_{pw} [*Ben-Menahem and Singh*, 1981; *Ichihara et al.*, 2012].

In practice, a suitable signal band pass must first be chosen, and the waveforms filtered, prior to applying cross correlation. Therefore, unless a large number of band passes are systematically searched, there is the potential to miss narrowband correlations between seismic and infrasonic waveforms that are otherwise uncorrelated at other frequencies. A significant practical advantage is thus made by also working in the frequency domain and using coherence in addition to cross correlation (see also the papers by *Sciotto et al.* [2011] and *Cannata et al.* [2013], who use coherence and wavelet transform coherence, respectively). We use the coherence (magnitude-squared coherence) between unfiltered seismic and acoustic waveforms:

$$\gamma_{wp}^2 = \frac{|S_{wp}|^2}{S_{ww}S_{pp}}, \tag{1}$$

where S_{ww} and S_{pp} are the power spectra of vertical seismic velocity and acoustic pressure, respectively, and S_{wp} is the cross spectrum. Additionally, we use the phase spectrum

$$\Phi_{wp} = \tan^{-1}\left(\frac{-Q_{wp}}{C_{wp}}\right), \tag{2}$$

where C_{wp} and Q_{wp} are the cospectrum and quadrature spectrum, i.e., the real and imaginary parts of S_{wp}, respectively.

We note that the characteristic $\pi/2$ phase shift for incident infrasound [*Ichihara et al.*, 2012] will only be observed when the seismic and infrasound sensors are perfectly collocated. However, this method relies on a small separation between the sensor pairs such that wind noise is uncorrelated. The sensor separation results in an additional time delay or phase shift, which can be removed for a known sensor pair geometry, back azimuth to the volcanic source, and apparent velocity (function of incidence angle and sound speed). We assume a plane wave for this correction [*DeFatta et al.*, 1988].

3. Applications to Volcano Seismoacoustic Data

3.1. Infrasound Array at Mount St. Helens, Washington

We apply this method to an infrasound array dataset from Mount St. Helens [*Matoza et al.*, 2007]. The data from the Coldwater (CDWR) array (13.4 km range) consist of a ~100 m aperture four-element broadband microbarometer array with a broadband seismometer a few meters from the central element. An advantage of these data is that array processing provides an independent method for identifying acoustic signals and separating them from seismic signals and mechanical shaking of the infrasound sensors [*Alcoverro et al.*, 2005], permitting validation of the method.

Figure 1 shows the coherence (equation (1)) and phase (equation (2)) spectra estimated in a 10 s sliding time window of unfiltered data for a phreatic explosion on 8 March 2005 [*Matoza et al.*, 2007]. The acoustic channel used is element two of the array, which is offset 51 m to the east and 14 m to the north of the seismometer. For comparison, we also display the cross-correlation (Figure 1d) function of 5–10 Hz filtered data, following the method described by *Ichihara et al.* [2012]. Note in Figure 1e that the coherence spectrogram provides a simple visualization of the frequency band pass in which the signals are coherent. The phase values for the eruption tremor signal (Figure 1f) are approximately $\pi/2$ after correcting for the propagation time delay. Note that an infrasound signal occurs at ~1150 s but is not from Mount St. Helens (Figure 1g). This signal from the wrong azimuth (185–190°) has accordingly different phase values (Figure 1f); thus, phase spectrograms such as Figure 1f provide useful source discrimination information if there is no infrasound array. However, having more sensor elements (i.e., an infrasound and/or seismic array) is preferable because of the azimuthal and phase ambiguity associated with a two-element seismic-acoustic sensor pair.

Figure 1e clearly shows that the seismic and acoustic data are coherent during the eruption in the band from ~5 Hz up to the Nyquist frequency of 20 Hz (anti-aliasing filter reduces signal above ~17 Hz). PMCC [*Cansi*, 1995] array processing results (Figure 1g) demonstrate conclusively that the signal recorded on the acoustic channel (Figure 1b) is an acoustic wave, i.e., propagating at acoustic velocity. Thus, the signal recorded on the seismometer in the band from ~5–17 Hz (Figures 1c and 1d) represents air-ground coupling, and is not generated by a subsurface seismic source.

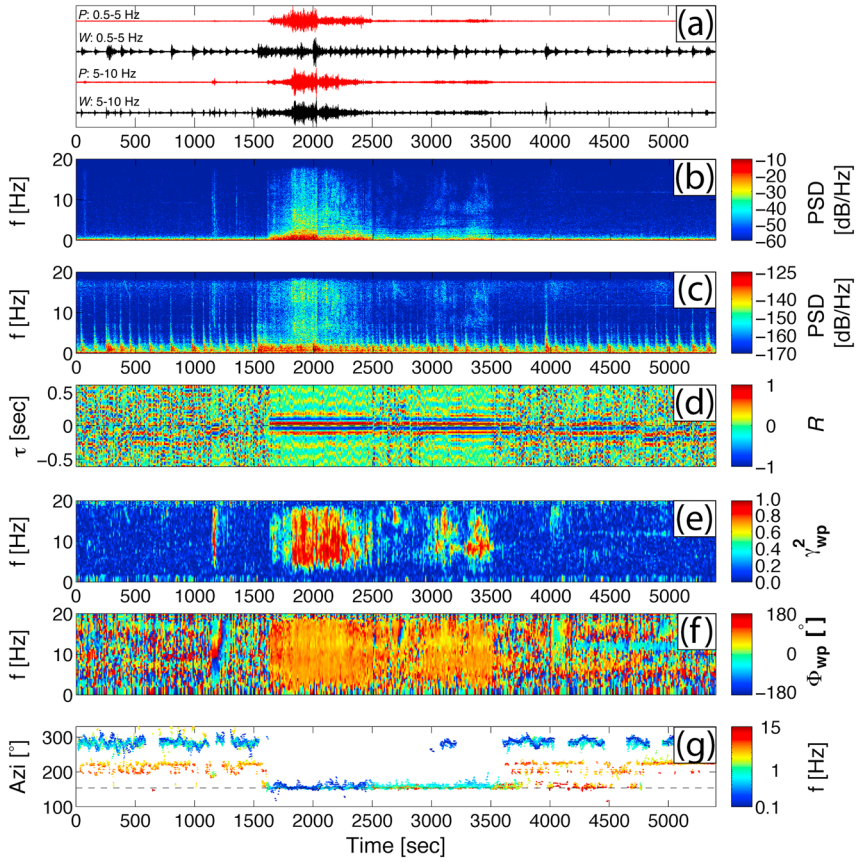

Figure 1. Time evolution of seismoacoustic spectra, cross-correlation, coherence, and cross-phase spectra for a sustained phreatic explosion on 8 March 2005 at Mount St. Helens recorded at CDWR (13.4 km range). (a) Red: infrasound pressure waveforms, black: vertical seismic velocity waveforms; upper two traces filtered 0.5–5 Hz, lower two traces filtered 5–10 Hz. (b) Infrasound spectrogram; decibel scale is for power spectral density (PSD) (Pa^2/Hz) re 1 Pa. (c) Seismic spectrogram; decibel scale is for PSD ($(m/s)^2$/Hz) re 1 m/s. (d) Cross correlation $R[\tau; W(t, \mathbf{x_s}), P(t, \mathbf{x_p})]$ in a 10 s sliding time window for 5–10 Hz filtered waveforms, following the method of *Ichihara et al.* [2012]. (e) Coherence and (f) phase spectrograms obtained by estimating γ^2_{wp} and Φ_{wp}, respectively, in a 10 s sliding time window on unfiltered data. (g) Progressive Multi-Channel Correlation (PMCC) array processing results for the four-element infrasound array, identifying acoustic signals from the direction of Mount St. Helens (black dashed line, 153°). Note that the infrasound signal at ~1150 s is not from Mount St. Helens (wrong azimuth).

Note that the seismic record (Figures 1a and 1c) also includes a series of repetitive long-period (LP) seismic events, which dominate below ~5 Hz. Beginning ~83 s before the acoustic signal arrives, the LPs merge closer in time during the eruption and generate a separate seismic component of eruption tremor [*Matoza and Chouet*, 2010]. Therefore, the seismic eruption tremor signal is a mix of (1) dominantly seismic energy below 5 Hz, transitioning into (2) air-ground coupled energy above 5 Hz. The acoustic signal is broadband from ~0.05–17 Hz, so only the portion of the signal >5 Hz couples effectively into the seismic record at a signal level above the repetitive LP events.

Finally, we note that the detection levels of the techniques are different. Infrasound array processing (Figure 1g) identifies a weak signal continuing from ~3500 s to ~4750 s, which can also be recognized in the cross-correlation pattern (Figure 1d). This weak signal is not visible in the coherence and phase spectra (Figures 1e and 1f).

3.2. Tungurahua, Ecuador

We apply a similar analysis to the 14–15 July 2006 eruption of Tungurahua, Ecuador, which was recorded with a similar sensor configuration as at Mount St. Helens, but at a greater distance of 36.9 km from the source [*Matoza et al.*, 2009; *Fee et al.*, 2010]. Figure 2 shows the cross correlation (Figure 2d) applied to 0.3–5 Hz filtered data, and the coherence and phase spectrograms (Figures 2e and 2f) in the 0–5 Hz band; note that seismic data >5 Hz are noisy and have been excluded. A broadband infrasound signal (Figure 2b)

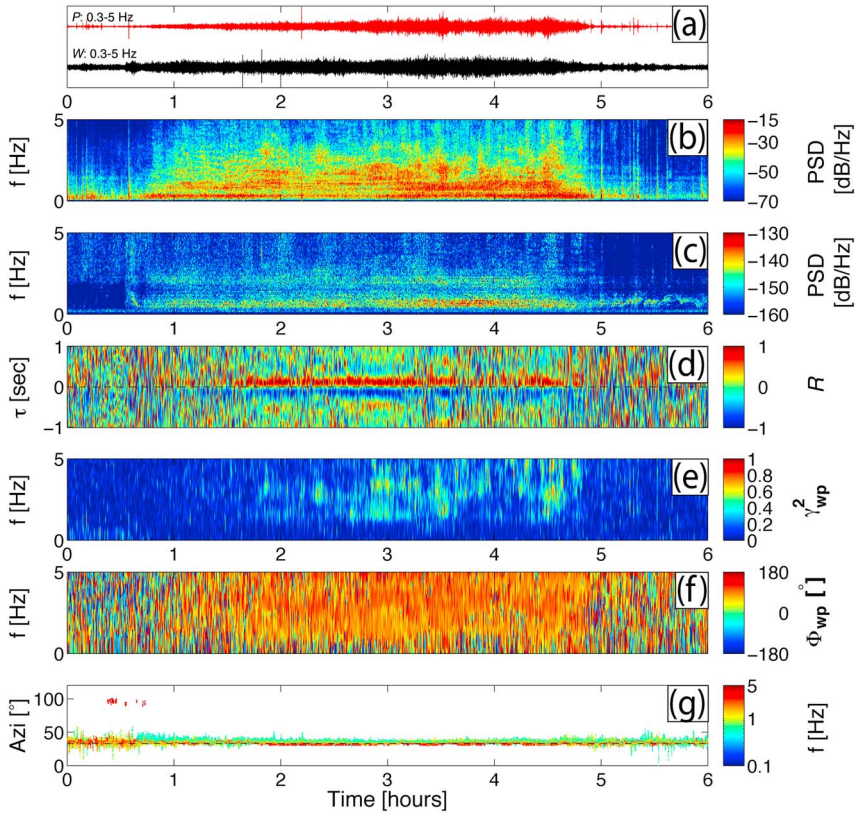

Figure 2. Similar analysis as shown in Figure 1 applied to the 14–15 July 2006 eruption at Tungurahua, Ecuador. (a) Acoustic (red) and seismic vertical velocity (black) data recorded at RIOE (36.9 km) filtered from 0.3 to 5 Hz. (b) Acoustic spectrogram. (c) Seismic spectrogram. (d) Cross correlation in a 20 s sliding time window for 0.3–5 Hz filtered waveforms. (e) Coherence and (f) phase spectrograms using the same 20 s sliding time window. (g) PMCC array processing results for the four-element infrasound array, identifying acoustic signals from the direction of Tungurahua (black dashed line, 33°).

is accompanied by banded seismic tremor (Figure 2c), with power concentrated between ~0.3 to 1.2 Hz and ~1.6 to 2.5 Hz. There is also banding in the infrasound data (Figure 2b), but there is not a simple correlation between the positions of bands in the infrasound and seismic signals.

Interestingly, coherence (Figure 2e) occurs, but at different frequencies from the banding in either case. In addition, the temporal variation of the ~0.3 to 1.2 Hz component of seismic eruption tremor is different from that of the infrasonic tremor. For example, (1) it begins with a drop in frequency after an explosion at ~0.55 h and (2) it continues with spectral variability after the infrasonic tremor signals stops at ~5 hours. Taken together, this indicates that the seismic eruption tremor (Figure 2c) recorded at ~36.9 km from the eruption is composed of a complex mix of both seismic waves propagating from a subsurface source at the volcano and air-ground coupled infrasound. The seismic component is also likely modified by significant propagation effects over the 36.9 km range. We note that at this distance, it is challenging with a single seismic station to attribute all of the seismic energy to the volcano. However, the overall timing and similarity of signal envelopes for infrasound and seismic data (Figure 2a), together with the infrasound array processing results (Figure 2g), help to reduce ambiguity.

3.3. Redoubt Volcano, Alaska

Applying the method to the 2009 Redoubt eruption, Alaska, provides a counter example to that of Mount St. Helens. The data used are from the Alaska Volcano Observatory (AVO) network. We performed a manual search through historical AVO eruptions that were recorded by collocated infrasound and seismic stations. In general, we found clipping to be a common problem with short-period seismic recordings of eruption tremor, e.g., clipping occurred on the seismometers collocated with an infrasound sensor for the 1999 subplinian eruption at Shishaldin [*Caplan-Auerbach and McNutt*, 2003] and for the 2006 Augustine eruption [*McNutt et al.*, 2010]. At Redoubt in 2009 (Figures 3a and 3b) clipping is not as big an

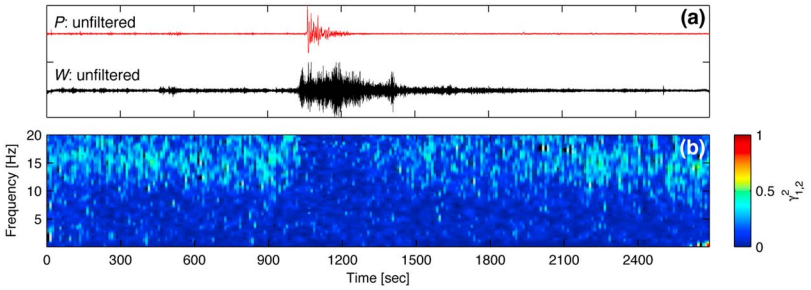

Figure 3. Lack of seismoacoustic coherence for eruption tremor at Redoubt Volcano, Alaska. (a) Forty-five minutes of unfiltered acoustic (red) and seismic (black) waveforms at DFR (12.2 km range) and (b) their coherence in 10 s sliding time windows for the 0702 UTC 23 March 2009 explosive event ("Event 2") [*McNutt et al.*, 2013]. Plot origin time is 0645 UTC 23 March 2009.

issue, but the acoustic and seismic sources appear to be distinct (different waveforms and poor coherence). A collocated short-period seismometer and Chaparral 25 acoustic sensor at station DFR, ~12.2 km from the vent, recorded strong eruption signals. Although seismic and acoustic amplitude envelopes are similar for multiple explosive events [*McNutt et al.*, 2013], we find poor waveform coherence at DFR, indicating that acoustic-seismic coupling from a subaerial source is not a dominant mechanism producing seismic eruption tremor at Redoubt.

4. Discussion and Conclusions: Acoustic and Seismic Components of Eruption Tremor

We have investigated examples of seismic eruption tremor containing varying degrees of infrasonic air-ground coupling. Mount St. Helens seismic eruption tremor (section 3.1), at 13.4 km range, is dominated by air-ground coupling from ~5–17 Hz; Tungurahua seismic eruption tremor (section 3.2), observed at a greater range of 36.9 km, contains a smaller component of air-ground coupling and the coupling results are more complex; and Redoubt seismic eruption tremor (section 3.3) is purely seismic. We conclude that air-ground coupling can occur in volcano-seismic installations and can be (although is not always) a significant component of eruption tremor. This should be considered in quantitative interpretation of seismic eruption tremor waveforms.

Figure 4 shows the coherence together with the gain $|\hat{g}|$ of the transfer function $\hat{g}$ for acoustic-seismic coupling for the Mount St. Helens data (section 3.1), where

$$\hat{g} = \frac{S_{wp}}{S_{pp}}. \tag{3}$$

The gain has values of between 1 and 10 μm·s^{-1}·Pa^{-1} (Figure 4b) in the frequency range of the coupling (5–17 Hz, Figure 4a), such that, e.g., an infrasound signal of 1 Pa would produce a seismic signal of 1–10 μm·s^{-1}. These gain values are consistent with previous observations of air-ground coupling [e.g., *Edwards et al.*, 2007, and references therein] and also agree (same order of magnitude) with acoustic-seismic coupling experiments at higher frequencies [*Sabatier et al.*, 1986]. Note that the gain increases with frequency (Figure 4b), which is likely dependent upon the near-surface geology [*Sabatier et al.*, 1986; *Madshus et al.*, 2005; *Hinzen*, 2007]. A similar analysis for the Tungurahua data (section 3.2), which we do not show here, leads to more complicated results because the air-ground coupled seismic signal and the true seismic signal have similar amplitudes, leading to a mixed signal.

Based on estimates of the transfer function of air-ground coupling at a given site from a given source, it may be possible to infer that the ground oscillation in a given frequency range is dominated by seismic waves rather than air-ground coupling, simply by considering amplitude envelopes [e.g., *Sciotto et al.*, 2011; *Ichihara et al.*, 2012]. For example, *Ichihara et al.* [2012] showed that the cross-correlation pattern disappeared when the seismic envelope grew and when the infrasound envelope decayed.

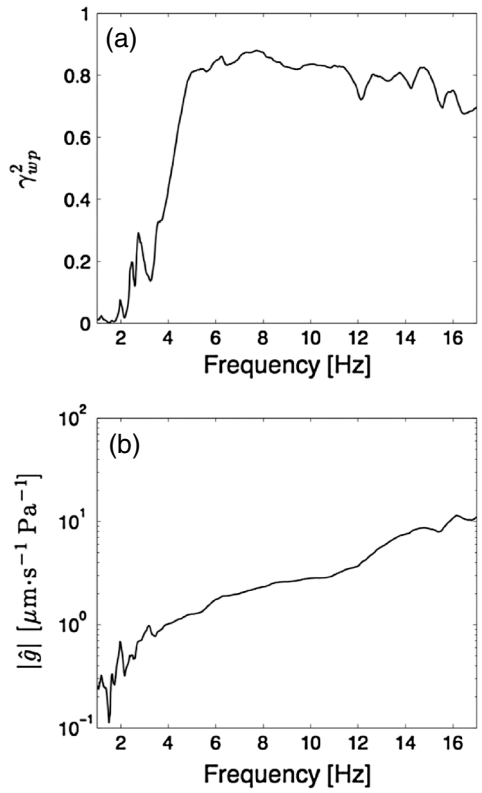

Figure 4. Multitaper estimates of the (a) coherence and (b) gain of the acoustic-seismic coupling for the 8 March 2005 Mount St. Helens data (from 1850 s to 2200 s in Figure 1).

Another approach to differentiating seismic and acoustic components of eruption tremor is to consider the moveout across a network [*Prejean and Brodsky*, 2011]. For the Mount St. Helens event analyzed in Figure 1, the >5 Hz component of eruption tremor (identified here as air-ground coupling) was also recorded on multiple stations across a local network [see *Moran et al.*, 2008, Figure 6]; thus, we hypothesize that air-ground coupling is not limited to the CDWR site. We attempted to assess the moveout of the >5 Hz signal across the seismic network in order to discriminate between acoustic and seismic propagation velocity; however, we found this difficult in practice because of the emergent nature of the eruption tremor signal and limited range over which the signal was recorded. A different approach to identifying acoustic components of eruption tremor is with seismic array analysis [*Nakamichi et al.*, 2013].

Our results indicate that air-ground coupling can occur from volcanic infrasound and that it can complicate volcano-seismic eruption tremor recordings, consistent with previous studies [*Ichihara et al.*, 2012; *Nakamichi et al.*, 2013]. We have not quantitatively investigated factors that influence the air-ground coupling mechanism, such as near-surface geology, frequency content, incidence angle, observation distance, seismometer burial depth, topography, etc. [e.g., *Madshus et al.*, 2005]. However, frequency-dependent near-surface geology site effects, range dependence, and incidence angle are likely important. For example, amplitudes of air-ground coupled phases recorded in the Lower Rhine Embayment from the Buncefield explosion, UK were a factor of 190 higher on stations on sediments compared to those on rock [*Hinzen*, 2007]. In addition, the differences in coupling results between Tungurahua (station at 36.9 km) and Mount St. Helens (station at 13.4 km) are partially attributable to the differences in range, given differences in seismic and acoustic geometrical spreading factors and the range dependence of infrasound air-ground incidence angle.

Our work reiterates the utility of joint infrasonic and seismic data for understanding wavefields generated by active volcanic processes [e.g., *Matoza et al.*, 2007]. Our work also builds on that of *Ichihara et al.* [2012] and *Cannata et al.* [2013] in showing that seismic-acoustic cross-correlation and cross-spectral analysis are useful for identifying infrasound when there is no infrasound array, with potential applications for large collocated seismoacoustic network datasets such as USArray [e.g., *Walker et al.*, 2011].

Acknowledgments
We thank Bob Parker for the multitaper cross-spectral program used in Figure 4. We are indebted to Mie Ichihara and an anonymous reviewer for critical comments that improved the paper. R.S.M. was supported by the Cecil H. and Ida M. Green Foundation at the Institute of Geophysics and Planetary Physics, Scripps Institution of Oceanography. D.F. was supported by the Geophysical Institute of the University of Alaska Fairbanks and NSF grant EAR-1113294.

The Editor thanks two anonymous reviewers for their assistance in evaluating this manuscript.

References

Alcoverro, B., P. Martysevich, and Y. Starovoit (2005), Mechanical sensitivity of the microbarometers MB2000 (DASE, France) and Chaparral 5 (USA) to vertical and horizontal ground motion, *Inframatics*, *9*, 1–10.

Ben-Menahem, A., and S. J. Singh (1981), *Seismic Waves and Sources*, Springer, New York.

Cannata, A., P. Montalto, and D. Patane (2013), Joint analysis of infrasound and seismic signals by cross wavelet transform: Detection of Mt. Etna explosive activity, *Nat. Hazard. Earth Syst. Sci.*, *13*, 1669–1677.

Cansi, Y. (1995), An automatic seismic event processing for detection and location: The P.M.C.C. method, *Geophys. Res. Lett.*, *22*(9), 1021–1024.

Caplan-Auerbach, J., and S. R. McNutt (2003), New insights into the 1999 eruption of Shishaldin volcano, Alaska, based on acoustic data, *Bull. Volcanol.*, *65*, 405–417.

Caplan-Auerbach, J., A. Bellesiles, and J. K. Fernandes (2010), Estimates of eruption velocity and plume height from infrasonic recordings of the 2006 eruption of Augustine Volcano, Alaska, *J. Volcanol. Geotherm. Res.*, *189*, 12–18, doi:10.1016/j.volgeores.2009.10.002.

Chouet, B. A., and R. S. Matoza (2013), A multi-decadal view of seismic methods for detecting precursors of magma movement and eruption, *J. Volcanol. Geotherm. Res.*, *252*, 108–175, doi:10.1016/j.jvolgeores.2012.11.013.

DeFatta, D. J., J. G. Lucas, and W. S. Hodgkiss (1988), *Digital Signal Processing: A System Design Approach*, John Wiley, New York.
Edwards, W. N., D. W. Eaton, P. J. McCausland, D. O. ReVelle, and P. G. Brown (2007), Calibrating infrasonic to seismic coupling using the Stardust sample return capsule shockwave: Implications for seismic observations of meteors, *J. Geophys. Res.*, *112*, B10306, doi:10.1029/2006JB004621.
Fee, D., M. Garces, and A. Steffke (2010), Infrasound from Tungurahua Volcano 2006–2008: Strombolian to Plinian eruptive activity, *J. Volcanol. Geotherm. Res.*, *193*, 67–81, doi:10.1016/j.jvolgeores.2010.03.006.
Firstov, P. P., and N. M. Kravchenko (1996), Estimation of the amount of explosive gas released in volcanic eruptions using air waves, *Volcanol. Seismol.*, *17*, 547–560.
Hinzen, K.-G. (2007), London fuel tank explosion recorded by short-period seismic stations at 500-km distance, *Seismol. Res. Lett.*, *78*(3), 383–388.
Ichihara, M., M. Takeo, A. Yokoo, J. Oikawa, and T. Ohminato (2012), Monitoring volcanic activity using correlation patterns between infrasound and ground motion, *Geophys. Res. Lett.*, *39*, L04304, doi:10.1029/2011GL050542.
Jellinek, M., and D. Bercovici (2011), Seismic tremors and magma wagging during explosive volcanism, *Nature*, *470*, 522–526, doi:10.1038/natures09828.
Johnson, J. B. (2003), Generation and propagation of infrasonic airwaves from volcanic explosions, *J. Volcanol. Geotherm. Res.*, *121*, 1–14.
Madshus, C., F. Løvholt, A. Kaynia, L. R. Hole, K. Attenborough, and S. Taherzadeh (2005), Air-ground interaction in long range propagation of low frequency sound and vibration—Field tests and model verification, *Appl. Acoust.*, *66*, 553–578.
Marchetti, E., M. Ripepe, D. D. Donne, R. Genco, A. Finizola, and E. Garaebiti (2013), Blast waves from violent explosive activity at Yasur Volcano, Vanuatu, *Geophys. Res. Lett.*, *40*, 5838–5843, doi:10.1002/2013GL057900.
Matoza, R. S., and B. A. Chouet (2010), Subevents of long-period seismicity: Implications for hydrothermal dynamics during the 2004–2008 eruption of Mount St. Helens, *J. Geophys. Res.*, *115*, B12206, doi:10.1029/2010JB007839.
Matoza, R. S., M. A. H. Hedlin, and M. A. Garces (2007), An infrasound array study of Mount St. Helens, *J. Volcanol. Geotherm. Res.*, *160*, 249–262.
Matoza, R. S., D. Fee, M. A. Garces, J. M. Seiner, P. A. Ramon, and M. A. H. Hedlin (2009), Infrasonic jet noise from volcanic eruptions, *Geophys. Res. Lett.*, *36*, L08303, doi:10.1029/2008GL036486.
McNutt, S., G. Thompson, M. West, D. Fee, S. Stihler, and E. Clark (2013), Local seismic and infrasound observations of the 2009 explosive eruptions of Redoubt Volcano, Alaska, *J. Volcanol. Geotherm. Res.*, *259*, 63–76.
McNutt, S. R. (1992), Volcanic tremor, in *Encyclopedia of Earth System Science*, vol. 4, edited by L. Brekhovskikh, Academic, San Diego, Calif.
McNutt, S. R. (2000), Seismic monitoring, in *Encyclopedia of Volcanoes*, edited by H. Sigurdsson, Academic Press, San Diego, Calif.
McNutt, S. R., and T. Nishimura (2008), Volcanic tremor during eruptions: Temporal characteristics, scaling and constraints on conduit size and processes, *J. Volcanol. Geotherm. Res.*, *178*, 10–18, doi:10.1016/j.jvolgeores.2008.03.010.
McNutt, S. R., G. Tytgat, S. A. Estes, and S. D. Stihler (2010), A parametric study of the January 2006 explosive eruptions of Augustine Volcano, using seismic, infrasonic, and lightning data, in *The 2006 eruption of Augustine Volcano, Alaska*, edited by J. A. Power, M. L. Coombs, and J. T. Freymueller, U. S. Geological Survey Professional Paper 1769. [Available at http://pubs.usgs.gov/pp/1769/]
Moran, S. C., P. J. McChesney, and A. B. Lockhart (2008), Seismicity and infrasound associated with explosions at Mount St. Helens, 2004–2005, in *A Volcano Rekindled: The Renewed Eruption of Mount St. Helens, 2004–2006*, edited by D. R. Sherrod, W. E. Scott, and P. H. Stauffer, U.S. Geological Survey Professional Paper 1750. [Available at http://pubs.usgs.gov/pp/1750/]
Nakamichi, H., Y. Yamanaka, T. Terakawa, S. Horikawa, T. Okuda, and F. Yamazaki (2013), Continuous long-term array analysis of seismic records observed during the 2011 Shinmoedake eruption activity of Kirishima volcano, southwest Japan, *Earth Planets Space*, *65*, 551–562.
Prejean, S. G., and E. E. Brodsky (2011), Volcanic plume height measured by seismic waves based on a mechanical model, *J. Geophys. Res.*, *116*, B01306, doi:10.1029/2010JB007620.
Sabatier, J., H. E. Bass, L. N. Bolen, and K. Attenborough (1986), Acoustically induced seismic waves, *J. Acoust. Soc. Am.*, *80*(2), 646–649.
Sciotto, M., A. Cannata, G. Di Grazia, S. Gresta, E. Privitera, and L. Spina (2011), Seismoacoustic investigations of paroxysmal activity at Mt. Etna volcano: New insights into the 16 November 2006 eruption, *J. Geophys. Res.*, *116*, B09301, doi:10.1029/2010JB008138.
Vergniolle, S., and J. Caplan-Auerbach (2006), Basaltic thermals and subplinian plumes: Constraints from acoustic measurements at Shishaldin volcano, Alaska, *Bull. Volcanol.*, *68*, 611–630.
Walker, K. T., R. Shelby, M. A. H. Hedlin, C. de Groot-Hedlin, and F. Vernon (2011), Illuminating infrasonic hot spots in the western U. S. with the USArray, *J. Geophys. Res.*, *116*, B12305, doi:10.1029/2011JB008579.